



Cite this: *Nanoscale*, 2016, 8, 15783

Selenium nanoparticles incorporated into titania nanotubes inhibit bacterial growth and macrophage proliferation

Wenwen Liu,^{a,b} Negar H. Golshan,^b Xuliang Deng,^{*a} Daniel J. Hickey,^b Katherine Zeimer,^b Hongyi Li^c and Thomas J. Webster^{*b,d}

Since implants often fail due to infection and uncontrolled inflammatory responses, we designed an *in vitro* study to investigate the antibacterial and anti-inflammatory properties of titanium dioxide nanotubes (TNTs) incorporated with selenium nanoparticles (SeNPs). Selenium incorporation was achieved by the reaction of sodium selenite (Na_2SeO_3) with glutathione (GSH) under a vacuum in the presence of TNTs. Two types of bacteria and macrophages were cultured on the samples to determine their respective anti-bacterial and anti-inflammatory properties. The results showed that the TNT samples incorporating SeNPs (TNT-Se) inhibited the growth of *Escherichia coli* and *Staphylococcus aureus* compared to unmodified TNTs, albeit the SeNP concentration still needs to be optimized for maximal effect. At their maximum effect, the TNT-Se samples reduced the density of *E. coli* by 94.6% and of *S. aureus* by 89.6% compared to titanium controls. To investigate the underlying mechanism of this effect, the expression of six *E. coli* genes were tracked using qRT-PCR. Results indicated that SeNPs weakened *E. coli* membranes (*ompA* and *ompF* were down-regulated), decreased the function of adhesion-mediating proteins (*csgA* and *csgG* were progressively down-regulated with increasing SeNP content), and induced the production of damaging reactive oxygen species (*ahpF* was up-regulated). Moreover, TNT-Se samples inhibited the proliferation of macrophages, indicating that they can be used to control the inflammatory response and even prevent chronic inflammation, a condition that often leads to implant failure. In conclusion, we demonstrated that SeNP-TNTs display antibacterial and anti-inflammatory properties that are promising for improving the performance of titanium-based implants for numerous orthopedic and dental applications.

Received 2nd June 2016,
Accepted 29th July 2016
DOI: 10.1039/c6nr04461a
www.rsc.org/nanoscale

Introduction

Novel materials are constantly being developed to improve medical device performance for regenerative medicine, tissue engineering, and drug delivery.¹ *In vitro* studies with these new materials have clearly shown that cells respond to nanoscale features on substrates, and have further elucidated the complex interplay between cells and their environment.² Titanium (Ti)-based materials have drawn great attention for orthopedic/dental applications due to their mechanical properties, biocompatibility, and the ease with which they can be modified at

the nanoscale.³ Titanium dioxide (TiO_2) nanotubes are one such nanostructure that have been demonstrated to induce significantly greater osteogenesis compared to unmodified Ti.⁴ Prepared by anodizing Ti under unique conditions, TiO_2 nanotubes (TNTs) have been reported to improve biomaterial performance and cytocompatibility, particularly for drug delivery applications.^{5,6} However, TNTs formed on the surface of Ti in an oxygen-containing environment may not exhibit antibacterial properties.⁷ Thus, just like unmodified Ti, TNTs and the tissues adjacent to TNTs, may be susceptible to bacterial infections.^{8,9}

The colonization of these implants by bacteria can lead to serious complications, including denture stomatitis during dental applications, characterized by an inflamed mucosa and resulting in extreme patient discomfort.¹⁰ Dentures are particularly susceptible to biofilm formation, which can be very difficult to eradicate, and often requires secondary procedures.¹¹ The bacterial-colonized implant or denture may also stimulate an inflammatory reaction, which then would be exacerbated in the presence of bacteria.

In efforts to provide Ti with antibacterial properties, some studies have doped antibacterial agents (such as gentamycin)

^aDepartment of Geriatric Dentistry, Peking University School and Hospital of Stomatology, Beijing 100081, PR China. E-mail: kqdengxuliang@bjmu.edu.cn; Fax: +86-10-82195581; Tel: +86-10-82195584

^bDepartment of Chemical Engineering, Northeastern University, Boston, MA 02115, USA. E-mail: th.webster@neu.edu; Fax: +1-617-373-6566; Tel: +1-617-373-6585

^cPhotoelectrochemical Research Group, Key Laboratory of Advanced Functional Materials, School of Materials Science and Engineering, Beijing University of Technology, Beijing, 100124, China

^dCenter of Excellence for Advanced Materials Research, King Abdulaziz University, Jeddah, Saudi Arabia

into TNTs.¹² Several studies have reported the promise of incorporating antibiotic-loaded biodegradable polymers into TNTs.^{13–15} However, such techniques to date have been limited, as the antibacterial agents incorporated into TNTs have short release times, and antimicrobial peptides are easily degraded under physiological conditions. Moreover, it is well documented that bacteria quickly develop resistance against the antibacterial drugs that have been developed to kill them.^{16,17} Thus, to provide extended antibacterial properties to TiO₂ without the use of antibiotics, researchers have focused on exploring different chemistries or features at the nanoscale.^{18–21}

Nanoparticles have increased surface area and therefore have increased interactions with biological targets (such as bacteria) compared with conventional, micron-sized particles.²² Moreover, nanoparticles can easily penetrate micron-sized bacterial membranes. Here, we focused on selenium (Se) nanoparticles due to their antibacterial potential.²³ For example, Se-enriched probiotics have been shown to strongly inhibit the growth of pathogenic *Escherichia coli* *in vivo* and *in vitro*.²⁴

In the human body, Se is essential for protecting cells and tissues against oxidative damage, and its supplementary use has been widely explored for many applications, including tissue engineering, oncology, and inhibiting bacteria, with low off-

target toxicity.^{22,25,26} Elemental Se is also required for the optimal functioning of the immune system, particularly in controlling the behavior of macrophages.²⁷ During an inflammatory reaction, uncontrolled macrophage recruitment and invasion play a central pathogenic role in certain chronic inflammatory lesions. Thus, controlling macrophage responses is critical in limiting the conditions of chronic inflammation and preventing implant failure. To address this problem, Se nanoparticles (SeNPs) could counteract chronic inflammation by influencing the macrophage signal-transduction pathways elicited by the bacterial endotoxin, lipopolysaccharide.²⁸

Here, we combined the osteogenic properties of TNTs with the antimicrobial and immunomodulatory traits of SeNPs in an attempt to regulate macrophage activity and reduce bacterial adhesion and growth on Ti-based medical devices, without the use of antibiotics.

Results and discussion

Substrate characterization

The diameter of the TNTs formed by anodization was ~125–150 nm, with a length of ~2 μm (Fig. 1A and E). When

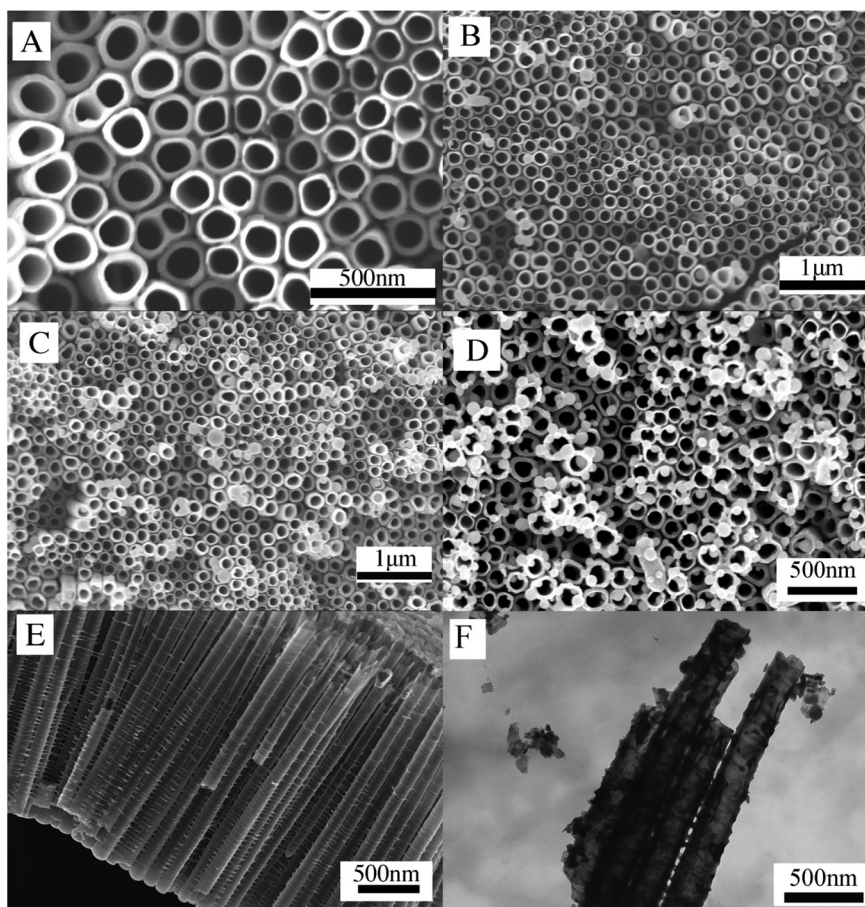


Fig. 1 SEM images of the samples. (A) Titanium nanotubes (TNTs). (B–D) TNTs incorporating Se at low: TNT-Se-L (B), medium: TNT-Se-M (C), and high: TNT-Se-H (D) concentrations. (E) Cross-section image of TNTs. (F) TEM image of cross-section of TNT-Se-M.

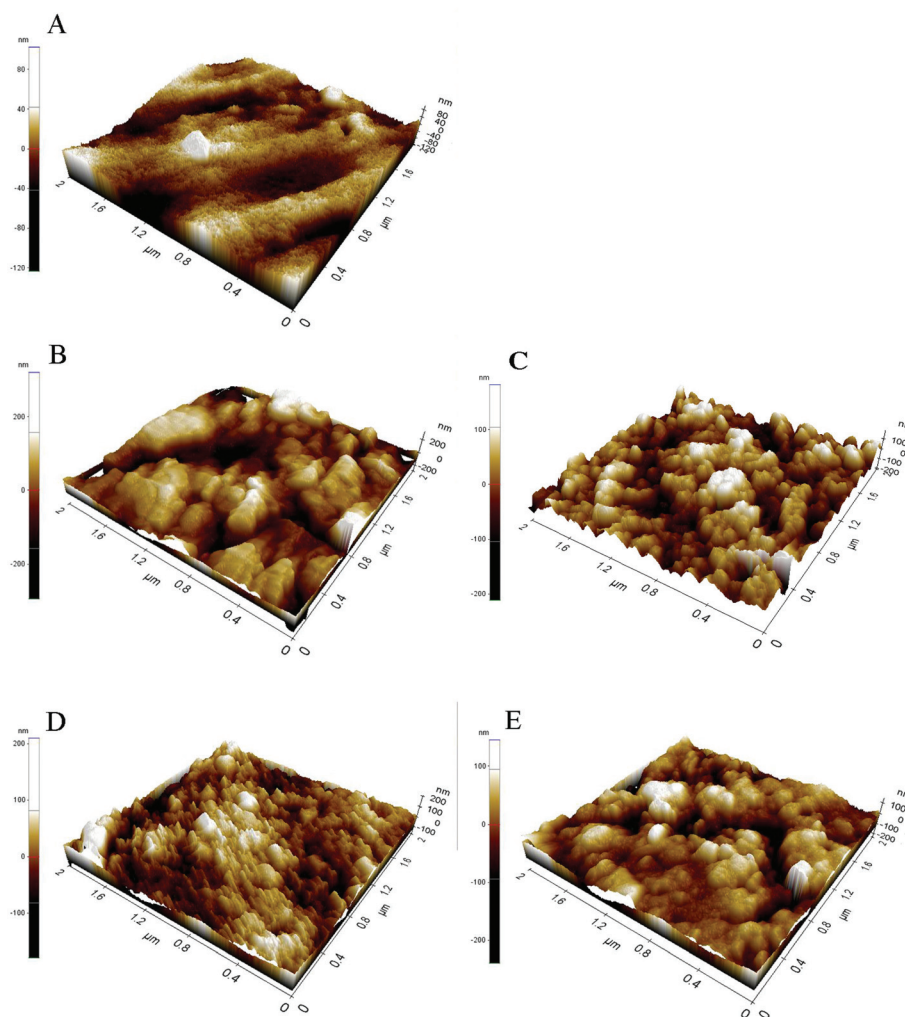


Fig. 2 AFM images of samples. (A) Ti. (B) Titanium nanotubes (TNTs). (C–E) TNTs incorporating Se at low: TNT-Se-L (C), medium: TNT-Se-M (D), and high: TNT-Se-H (E) concentrations.

Table 1 Surface energy of samples (mJ m^{-2})

	Ti	TNTs	TNTs-Se-L	TNTs-Se-M	TNTs-Se-H
Surface energy without UV	4.33 ± 0.75	58.36 ± 0.30	66.19 ± 1.88	62.66 ± 0.61	62.49 ± 2.97
Surface energy with UV treatment	7.9 ± 0.96	70.88 ± 0.75	66.68 ± 0.52	67.54 ± 1.17	63.25 ± 0.66

After UV light exposure, all TNT-Se sample contact angles were reduced and the surface energy increased. TNT-Se-L, M, and H: TNTs incorporating Se at low, medium, and high concentrations. Data are expressed as the mean \pm standard deviation ($n = 3$).

doped into the TNTs, the SeNPs appeared spherical, with diameters ranging from 20 to 100 nm (Fig. 1B–D and F). Samples were named according to the amount of SeNPs doped into TNTs as TNT-Se-L, TNT-Se-M, and TNT-Se-H (where L, M, and H stand for low, middle, and high Se concentrations). The amount of SeNPs embedded into TNTs was controlled by the reagent concentrations.

Atomic force microscope images showed that the surfaces of all samples had similar root mean squared (rms) roughness values of 110–150 nm (Fig. 2). The surface energies of

samples with and without UV treatment are shown in Table 1. Increased surface energies were measured after the conversion of plain Ti into TNTs (and TNT-Se).

Chemical composition and crystal structure

Energy dispersive X-ray spectrometry confirmed that the basic elements present were Ti, O, and Se. The X-ray diffraction (XRD) spectra of the samples displayed Ti and anatase TiO_2 peaks for both the TNT and TNT-Se samples (Fig. 3). Some small peaks in the rutile phase were also detected in the XRD

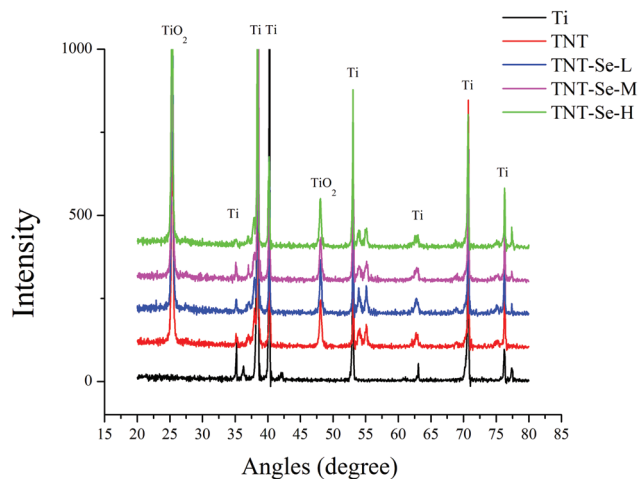


Fig. 3 XRD patterns of Ti, titanium nanotubes (TNTs), and TNTs incorporating Se at low (TNT-Se-L), medium (TNT-Se-M), and high (TNT-Se-H) concentrations.

for both kinds of samples. The TNT-Se samples showed slight changes in XRD, but there were no feature peaks for the Se compounds, most likely because the Se concentration was below the detection limit.

Further, X-ray photoelectron spectroscopy (XPS) revealed the presence of Ti, O, and Se in all of the TNT-Se samples (Fig. 4A). The C-bonding states on both the TNT and TNT-Se samples were consistent, and carbon was present even after 40 min of 2 kV Ar⁺ etching (Fig. 4B), suggesting that any carbon contamination was a part of the TNTs. In addition, there was no quantifiable change in the bonding states of the Ti 2p₃ or the O 1s before and after nanoparticle incorporation.

The Se dose in the TNTs was adjusted by controlling the reagent concentrations for the Se reaction in the TNTs, and XPS was used to quantify the relative atomic percentage of Se (Table 2). The overall percentage increased from <1% to 4 ± 0.5% for TNTs-Se-L to TNTs-Se-H, and the Se bonding states remained unchanged. The presence of Se after a 40 min etch suggests that the SeNPs were embedded into the TiO₂ nanotube structure.

Lastly, inductively coupled plasma atomic emission spectrometry showed the Se release kinetics in phosphate-buffered saline (PBS) (Fig. 5). The amounts of Se released corresponded with the original Se embedding level, and the accumulated amount of Se released into PBS increased steadily during the 30-day duration of the study, suggesting that the embedded Se could have controllable long-term therapeutic effects as it is released from TNTs.

TNT-Se samples display antibacterial efficacy

All TNT-Se samples significantly decreased both *E. coli* and *S. aureus* density compared to control Ti samples at all time points during the 30-day duration of the study, with the exception of *S. aureus* at day 30 (Fig. 6A and B). Interestingly, TNTs had a greater concentration of bacteria than unmodified Ti,

perhaps due to increases in surface area. The TNT-Se-H sample had the lowest number of bacteria during the first 7 days compared to all other samples ($p < 0.05$). For *E. coli*, TNT-Se-H, TNT-Se-M, and TNT-Se-L supported similar numbers of bacteria after days 15 and 30, possibly because the rate of Se release became similar in the three samples. At the same time, bacteria numbers increased on all TNT-Se samples, suggesting that the dynamic interaction of SeNPs and the micro-environment created by the bacteria could lead to the release of soluble Se species which could decrease Se content on TNT with prolonged culture times. *E. coli* has an electrostatic repulsion to the negative charge of SeNPs which can protect *E. coli* from the reactive oxygen species (ROS) created by SeNPs.^{26,29} In our study, the concentration of SeNPs may not have been enough to overcome the resistance of *E. coli* after 15 days. Compared to *E. coli*, *S. aureus* is a Gram-positive bacteria whose net surface charge is considerably less negative than for Gram-negative bacteria. Thus, *S. aureus* was more initially sensitive to SeNPs than *E. coli*. However, after 30 days, the number of *S. aureus* was not significantly different on Ti and TNT-Se samples, which meant that the SeNPs content decreased to the lower limit to inhibit the growth of *S. aureus*. Further optimization is clearly needed in terms of SeNP concentration and localization of SeNP to maximize *S. aureus* inhibition. However, the bacteria numbers on the TNT-Se samples were still lower than those on TNTs. The greatest decrease in bacterial growth on the TNT-Se samples were 94.6% for *E. coli* after day 5 and 89.7% for *S. aureus* after day 7 (calculated from the formula: $(A - B)/A \times 100\%$, where A is the number of bacteria in the control group and B is the number of bacteria in the experimental group). Similar trends in the growth of *E. coli* and *S. aureus* indicated that TNT-Se samples could be effective in resisting both Gram-negative and Gram-positive bacteria growth, which is impressive when using the same treatment process.

Bacteria grown on all samples were also visualized using scanning electron microscopy (SEM) (Fig. 7 and 8). The electron micrographs showed that *E. coli* had intact membranes on both the untreated Ti and TNTs (Fig. 7A and B). In contrast, the membranes of *E. coli* grown on TNT-Se samples became corrugated. Some SeNPs had even adsorbed onto and disrupted the *E. coli* membranes (Fig. 7D). It is not yet clear whether this bacteria-SeNP contact is necessary to induce membrane damage, and further studies are needed to elucidate this interaction. Similarly, *S. aureus* grown on Ti and TNTs were smooth and intact with typical spherical shapes (Fig. 8A and B). In contrast, the membranes of *S. aureus* on the TNT-Se-M substrate were corrugated and even ruptured where in contact with SeNPs (Fig. 8D).

Then, the ability of the samples to prevent bacterial growth was visualized and qualitatively assessed by confocal fluorescence microscopy and laser scanning cytometry (Fig. 9). After 24 h in culture, there were more live bacteria on Ti and TNT surfaces than the other samples, and the number of bacteria decreased as the Se content increased in the TNT-Se samples (Fig. 9A and B). The laser scanning (LSC) images

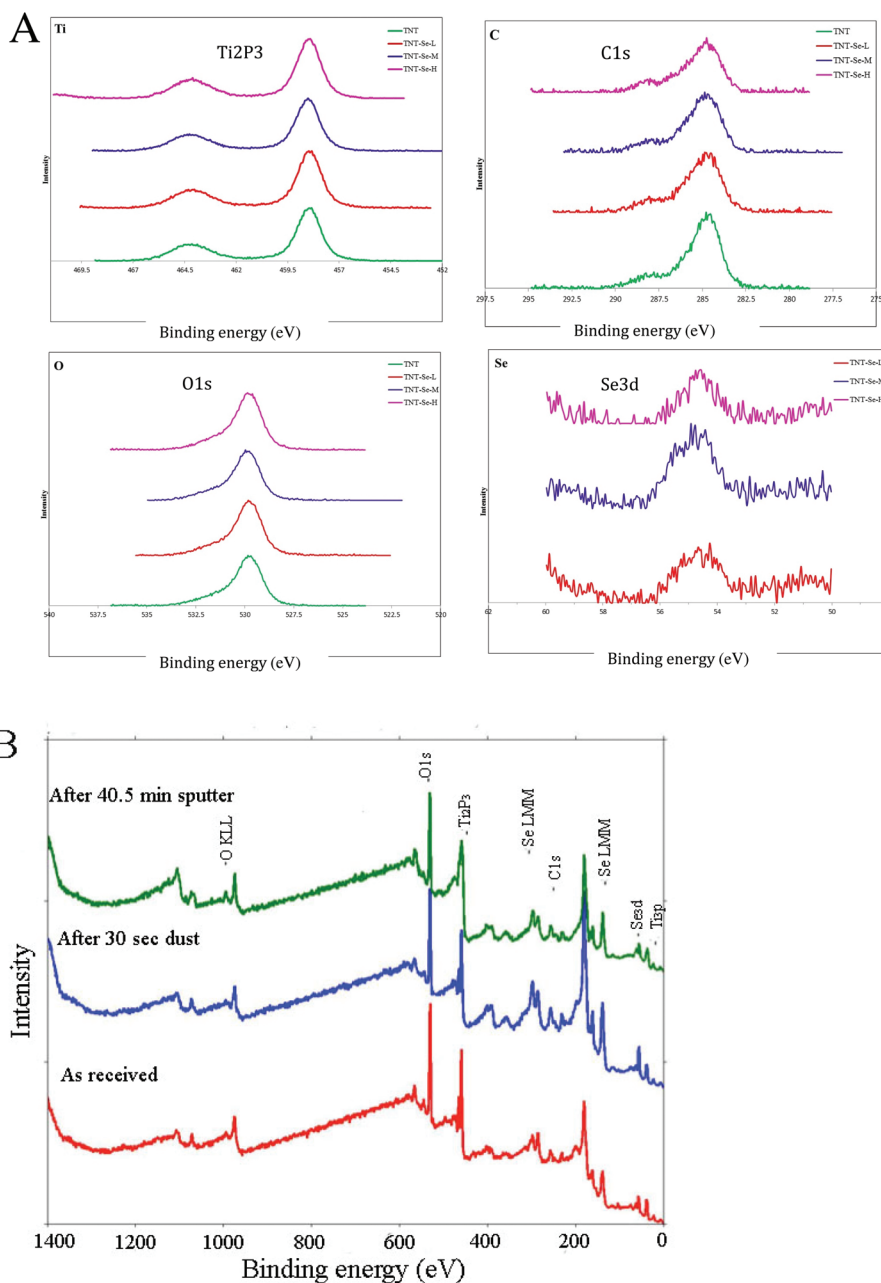


Fig. 4 (A) XPS spectra of elements in samples. (B) XPS spectra of TNT-Se-M at the indicated depths, sputter velocity: 1 nm min^{-1} (monochromatic Al source 2 kV Ar etch).

Table 2 Elemental composition of each sample, determined by XPS

	TNTs	TNT-Se-L	TNT-Se-M	TNT-Se-H	TNT-Se-M ^a (after 40.5 min sputter)
C 1s	14%	14%	13%	12%	5%
O 1s	66%	72%	63%	61%	52%
Se 3d5	0.00%	1%	2%	4%	Less than 1% (0.70%)
Ti 2p3	20%	13%	22%	23%	42%

TNT-Se-L, M, and H: TNTs incorporating Se at low, medium, and high concentrations. ^a Sputter velocity: 1 nm min^{-1} .

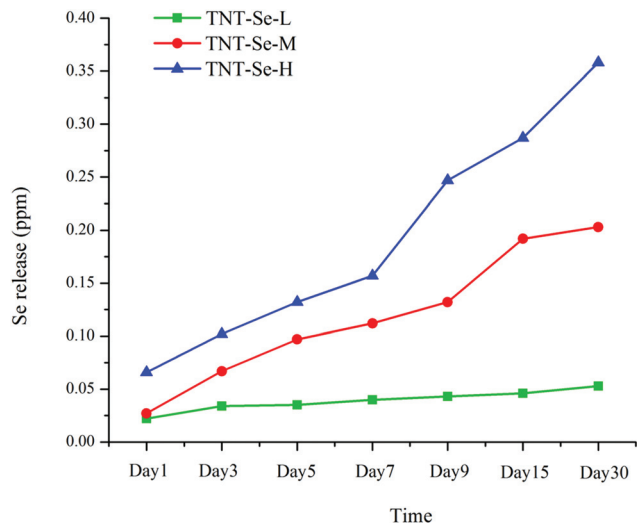


Fig. 5 Profiles of Se release from samples: cumulative concentrations. TNT-Se-L, M, and H: TNTs incorporating Se at low, medium, and high concentrations.

(Fig. 9C and D), which showed the entire surface area of samples, confirmed the confocal results, which also were in line with the quantitative data presented in Fig. 6.

Therefore, the results of this study prove that TNT-Se samples reduced bacterial colonization, and SeNPs had a direct affect in damaging both Gram-negative and Gram-positive bacteria that did attach to the TNT-Se samples (Fig. 6D and 7D). Thus, the mechanisms underlying these novel antibacterial properties of TNT-Se samples may include direct action *via* attraction and membrane damage.

TNT-Se samples increase reactive oxygen species (ROS) levels

The ROS generated in the bacteria (cultured in TSB) was determined in terms of malondialdehyde (MDA) equivalents using the Thiobarbituric Acid Reactive Substances Assay (TBARS) (Fig. 10). Increases in the number of MDA equivalents corresponded to increases in the amount of SeNPs in the TNTs. Furthermore, increases in the MDA equivalents also correlated with increases in the antibacterial effect, suggesting that this effect may be ROS-mediated. This mode of bacterial toxicity typically manifests as membrane lipid peroxidation leading to increased porosity.³⁰ The badly-damaged bacterial membranes observed *via* SEM (Fig. 7 and 8) support this hypothesis. In addition, it is possible that the effect of ROS production from SeNPs is enhanced as the SeNPs adhere to bacterial membranes.

TNT-Se samples affect *E. coli* gene expression

The expressions of six *E. coli* genes (*ompA*, *ompF*, *csgA*, *csgG*, *ahpF*, and *katG*) were determined for the samples of interest after 24 h of culture (Fig. 11). The results showed that *ompA* was down-regulated on TNT-Se samples, and *ompF* was increasingly down-regulated with increased Se content in the samples. OmpA is a major protein in the outer membrane of

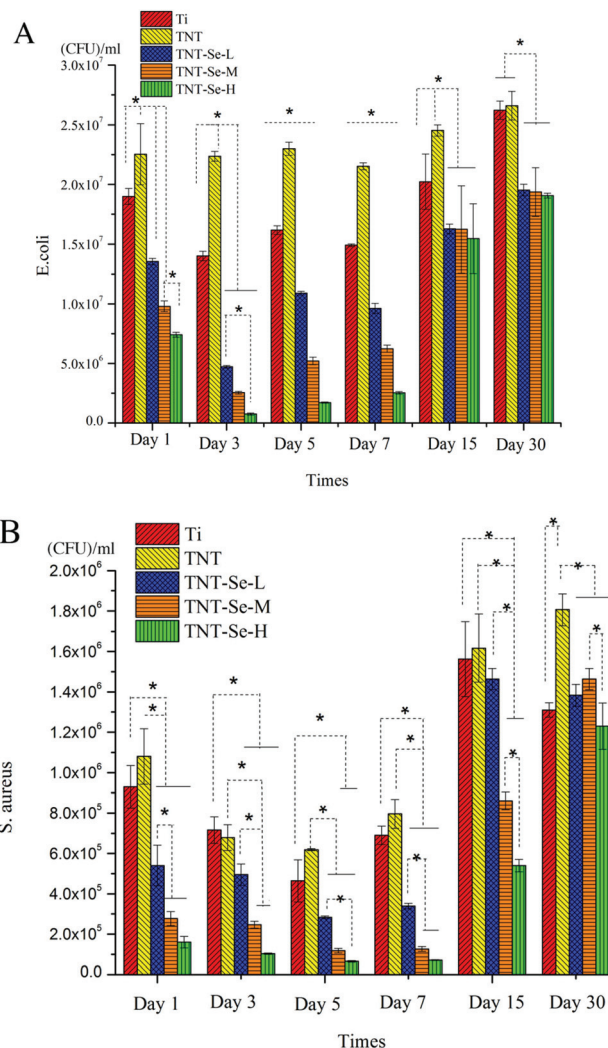


Fig. 6 (A) *E. coli* and (B) *S. aureus* on different samples, TNT-Se-L, M, and H: TNTs incorporating Se at low, medium, and high concentrations. Antibacterial assay data are expressed as the mean \pm standard deviation; ($n = 3$); * $p < 0.05$.

E. coli and is mainly associated with maintaining the structural integrity and the shape of the bacterium, although it also acts as a receptor for several bacteriophages and bacteriocins.³¹ The OmpA protein produces a diffusion channel allowing a slow penetration of small solutes, serves as an adhesin/invasin as well as an immune evasin, and is known to play a role in biofilm formation.^{32,33} OmpA may repair cell membrane damage to improve phenylpropanoid tolerance, and OmpF might function as a porin to allow the exit of antibacterial drugs.³⁴ OmpF porin channels are responsible for the passage of small hydrophilic solutes across the outer membrane of *E. coli*.³⁵ The down-regulation of *ompA* on TNT-Se samples indicates that the SeNPs may interfere with the structure or diffusion properties of *E. coli*, and the down-regulation of *ompF* may damage the ability to pump out antibacterial agents. Taken together, *E. coli* exposed to SeNPs may experience weakened membrane functions leading to cell death.

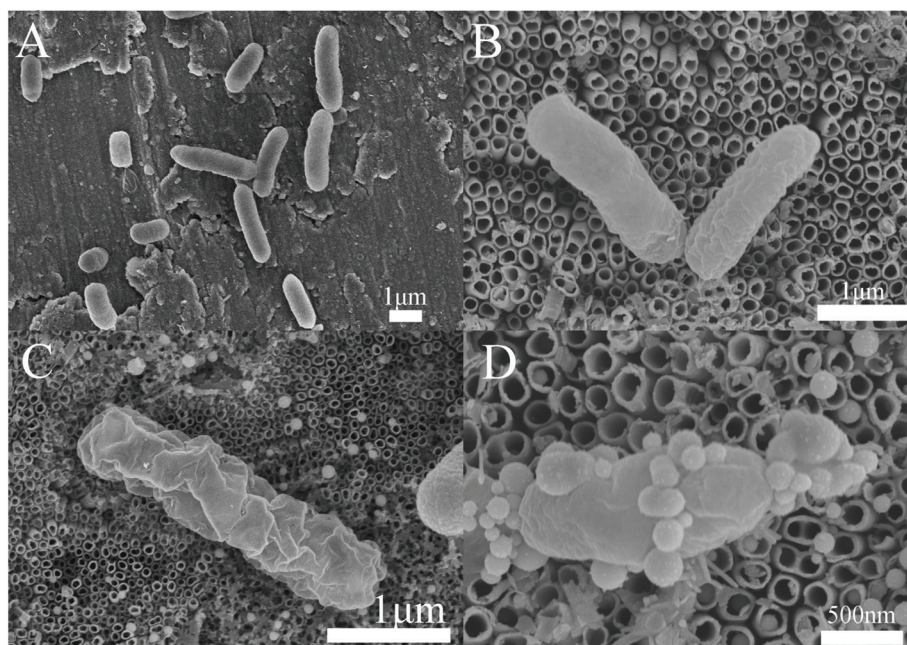


Fig. 7 Scanning electron micrographs of *E. coli* grown on samples of Ti (A), TNT (B), and TNT-Se-M (C, D). Note that released SeNPs adhered onto the bacterium in (D). TNT-Se-M: TNTs incorporating Se at medium concentrations.

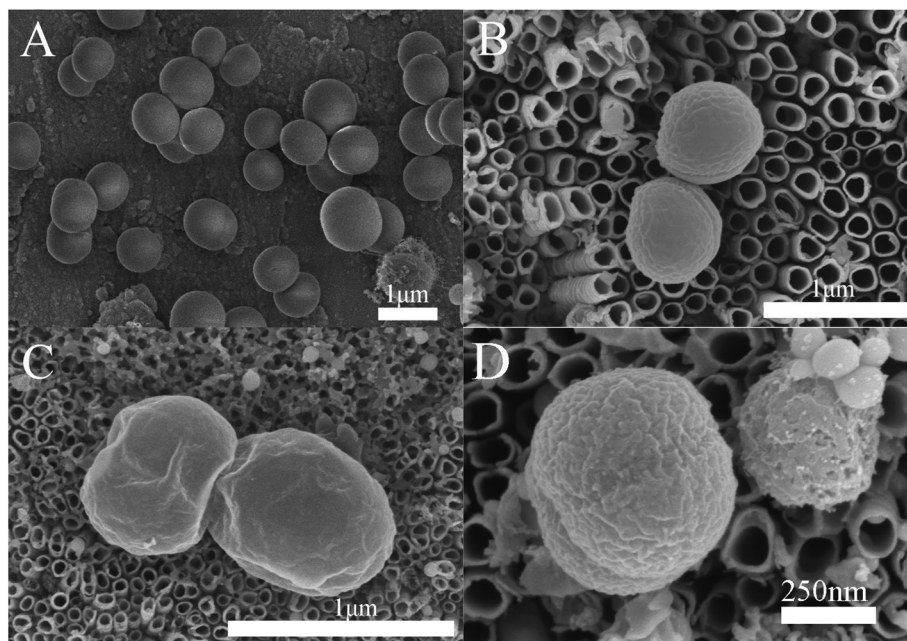


Fig. 8 Scanning electron micrographs of *S. aureus* grown on samples of Ti (A), TNT (B), and TNT-Se-M (C, D). Note that released SeNPs adhered onto the bacterium in (D). TNT-Se-M: TNTs incorporating Se at medium concentrations.

csgA and *csgC*, two genes encoding *E. coli* curli production, were down-regulated on TNT-Se-H samples. Curli are thin, coiled structures expressed on the surface of *E. coli* that mediate binding between cells and to various surfaces *via* a variety of extracellular matrix and serum proteins, such as soluble fibronectin, laminin, plasminogen, and plasminogen

activator proteins.^{36–38} CsgA (the major fiber subunit) and CsgG are non-structural proteins involved in curli biogenesis,³⁹ where CsgG (the outer membrane-located lipoprotein) is required for the stable maintenance of CsgA and CsgB levels.⁴⁰ In our study, both *csgA* and *csgG* were up-regulated slightly on TNT, TNT-Se-L, and TNT-Se-M samples, suggesting that the

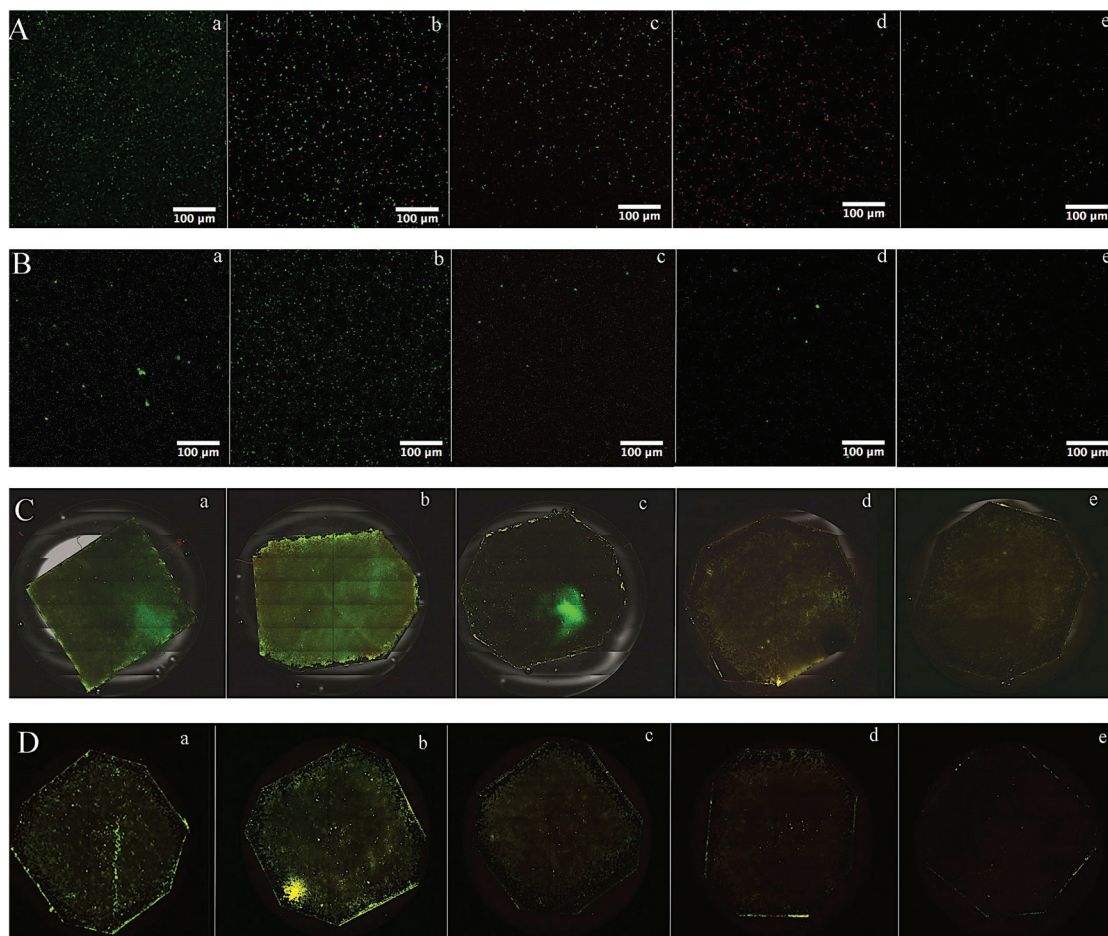


Fig. 9 (A, B) Fluorescence images showing the viability of *E. coli* (A) and *S. aureus* (B) on samples of (a) Ti, (b) TNT, (c) TNT-Se-L, (d) TNT-Se-M, and (e) TNT-Se-H. (C, D) Laser scanning cytometer images of *E. coli* (C) and *S. aureus* (D) on samples of (a) Ti, (b) TNT, (c) TNT-Se-L, (d) TNT-Se-M, and (e) TNT-Se-H. Live bacteria appear green (SYTO 9) while dead ones appear orange (propidium iodide). TNT-Se-L, M, and H: TNTs incorporating Se at low, medium, and high concentrations.

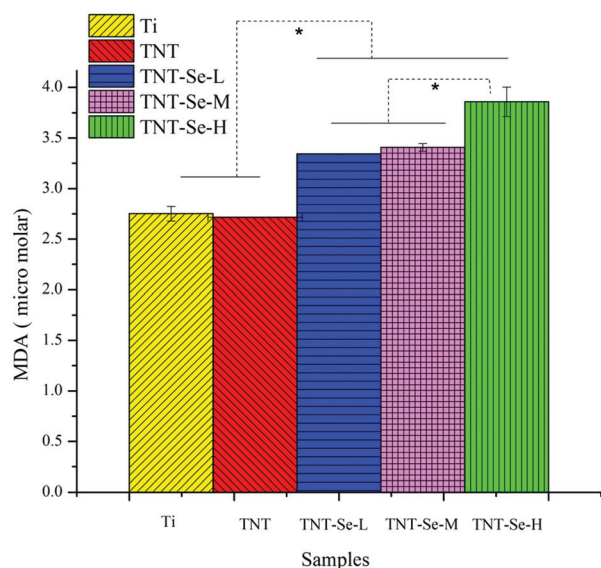


Fig. 10 Malondialdehyde (MDA) assays showing the ROS concentrations generated by *E. coli* cultured on the samples in TSB. TNT-Se-L, M, and H: TNTs incorporating Se at low, medium, and high concentrations. * $p < 0.05$.

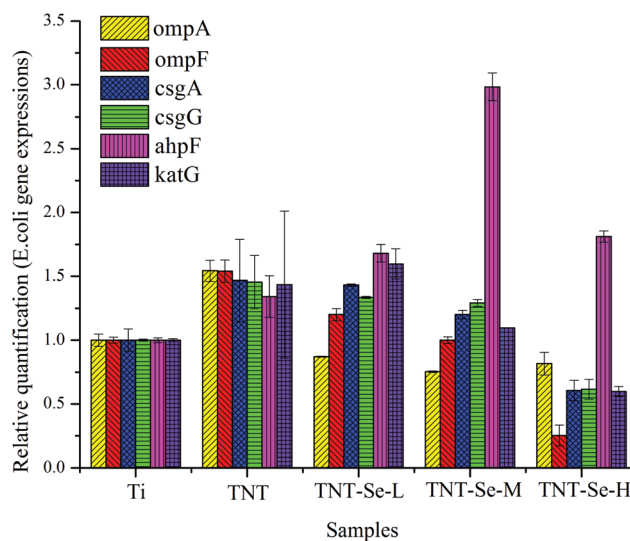


Fig. 11 *E. coli* gene expression on Ti, TNT and TNT-Se samples. TNT-Se-L, M, and H: TNTs incorporating Se at low, medium, and high concentrations. Data are expressed as the mean \pm standard deviation ($n = 3$).

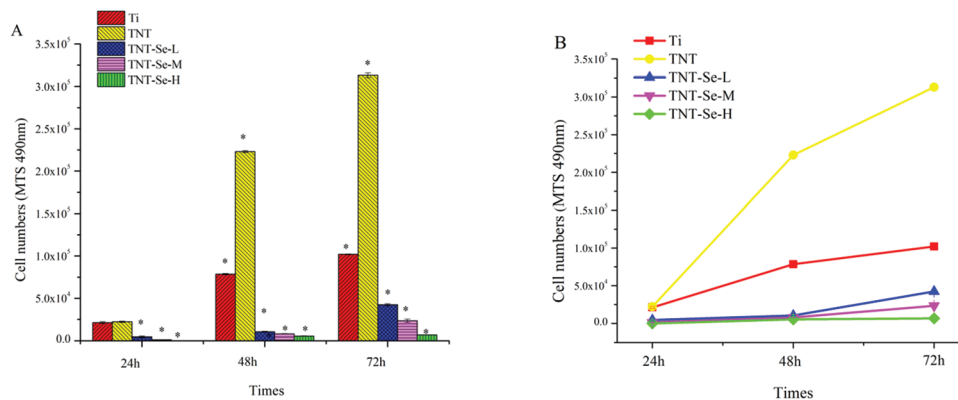


Fig. 12 Macrophage proliferation on samples. (A) MTS results from macrophage culture for 24, 48, and 72 h. (B) Macrophage proliferation on samples over 72 h of culture. Data are expressed as the mean \pm standard deviation; ($n = 3$); * $p < 0.05$ compared to all others at the same time point and with respect to the same sample previous time point.

nanotubular structure of TNTs increased curli expression. However, *csgA* and *csgG* were both down-regulated further as the Se content increased to TNT-Se-H, indicating that SeNPs may inhibit curli formation, thereby decreasing the adhesiveness of *E. coli*.

ahpF, which is responsible for encoding alkyl hydroperoxide reductase, was greatly up-regulated on the TNT-Se samples, especially on TNT-Se-M. *katG*, encoding hydroperoxidase I, had the highest expression on TNT-Se-L, and decreased as the Se content increased. The *katG* and *ahpF* genes are involved in the *E. coli* system for sensing and removing endogenous and exogenous oxidants.⁴¹ It has been reported⁴² that these genes are frequently overexpressed as part of a transcriptional strategy against the deleterious effects of peroxides, and several authors⁴³ have claimed that AhpF and KatG have a compensatory interaction. In our study, SeNPs were found to induce the production of ROS in bacteria, which stimulates the bacteria to react to this destructive factor. Both *ahpF* and *katG* were up-regulated slightly on TNT samples, possibly because there were more (ROS-producing) bacteria on TNTs than other samples. On all of the TNT-Se samples, *ahpF* was up-regulated, indicating that indeed the bacteria altered their gene expression in response to the increased ROS levels induced by exposure to SeNPs. *katG* was slightly down-regulated, which may have occurred as a compensatory response to *ahpF*. On TNT-Se-H samples, the *E. coli* were significantly inhibited, which may have contributed to the relatively decreased expression of *ahpF* compared to TNT-Se-M samples. Ultimately, it became clear that the TNT-Se samples attack bacteria by at least three pathways: disruption of membrane functions, damage to the production of adhesion-mediating proteins, and production of damaging ROS.

TNT-Se samples inhibit macrophage proliferation

After 24, 48, and 72 h, macrophages seeded onto TNT-Se samples had lower metabolic activity than cells seeded onto Ti and TNT samples (Fig. 12). Further, macrophage activity decreased with increasing SeNP content. This result is supported by evidence that Se suppresses LPS-induced nitric oxide

production and alleviates pathological conditions including inflammation.²⁸ Macrophages, a class of myeloid leukocyte with phagocytic activity and inflammatory signaling properties, play a pivotal role in antimicrobial defense and tissue homeostasis.⁴⁴ However, uncontrolled cytokines and inflammatory mediators may lead to excessive, even self-destructive cellular responses, which can be detrimental to dental/orthopedic implants. A possible mechanism for the anti-inflammatory activity of SeNPs is decreased cellular nitric oxide production caused by blocking NF-KB and inhibiting the phosphorylation of the JNK and p38 MAPK signal pathways, as reported by Wang *et al.*⁴⁵

While limiting macrophage proliferation is promising for controlling chronic inflammation, it is important to note that SeNPs have shown low cytotoxicity towards other cell types that are important for the proper integration of implants with surrounding tissues. For example, fibroblasts remained more than 70% viable when exposed to Se concentrations as high as 128 ppm,²⁹ and human embryonic kidney cells retained over 80% viability when exposed to SeNPs at concentrations greater than 100 $\mu\text{g mL}^{-1}$.²⁶ Thus, by incorporating SeNPs, TNTs may be able to control macrophage proliferation with low toxicity to other cells.

Materials and methods

Sample preparation and characterization

Preparation of TNTs. Pure titanium sheets (Sigma-Aldrich, St. Louis, MO, 10 \times 10 \times 0.3 mm³) were used as the starting material for all samples. Anodization was then carried out at 60 V for 2 h to create TNTs on the surface of Ti sheets. The anodization parameters used were the same as in our previous study.¹⁸

Incorporation of Se nanoparticles into TNTs. The annealed TNT samples were immersed in an aqueous solution containing sodium selenite (Na₂SeO₃) (99%, Alfa Aesar, Ward Hill, MA) and glutathione (GSH) (97%, TCI America, Portland, OR) at a 1 : 4 molar ratio in 50 ml tubes (Table 3). Sodium

Table 3 SeNP synthesis reagents and volumes

	TNT-Se-L (ml)	TNT-Se-M (ml)	TNT-Se-H (ml)
H ₂ O	29	18	2
GSH (100 mM)	0.5	6	14
Na ₂ SeO ₃ (25 mM)	0.5	6	14
Final volume	30	30	30

TNT-Se-L, M, and H: TNTs incorporating Se at low, medium, and high concentrations.

hydroxide (NaOH) (1 mol L⁻¹, Alfa Aesar, Ward Hill, MA) was added into the mixture to bring the pH into the alkaline region and initiate the reaction at room temperature. Immediately following the addition of NaOH, the tubes were placed into a container under vacuum for 1 min until the solution changed color, signifying that SeNPs had formed. All samples were rinsed five times in deionized water and then were soaked in deionized water for 24 h to remove any non-adherent SeNPs and possible remaining reactants. Finally, all the samples were exposed to UV light for 1 h before use in experiments.

Sample characterization. The surface morphologies of pure Ti, TNTs, and TNT-SeNPs were observed using field-emission scanning electron microscopy (S-4800 Cold Emission FE-SEM, Hitachi, Japan) and atomic force microscopy (AFM, NX-10, Park Systems, Suwon, Korea) with non-contact cantilever probes (PPP-NCHR, Park Systems).

Transmission electron microscopy (TEM, JEM-2100F, JEOL, Japan), X-ray diffraction (XRD, Philips X'Pert PRO, MA, USA), and energy-dispersive X-ray spectrometry (EDS; Hitachi, Japan) were used to probe the phase, composition, and distribution of SeNPs on TNTs.

X-ray photoelectron spectroscopy (XPS, Phi, Lake Drive East Chanhassen, MN) was used to determine the elemental composition and bonding states of the samples. The XPS consists of a dual source, non-monochromatic X-ray source (Phi model 04-548) and a hemispherical analyzer (Phi model 10-360). The two X-ray options were Mg K α (1253.6 eV) and Al K α (1486.6 eV) operated at 300 W. The system was calibrated using Au 4f and Cu 2p, and had a minimum full width at half-maximum of 1.5 eV with an 80% Gaussian/Lorentzian distribution at a pass energy of 35.75 eV. Background subtraction was performed using the integrated Shirley method.

Water contact angle measurements were carried out with a contact analysis system (Phoenix 300 Touch, Seoul, Korea). The surface free energy of each sample was then determined from the corresponding contact angle measurement.

To monitor the amount of Se released from the samples over time, the TNT-Se samples were immersed in 4 mL of phosphate-buffered saline (PBS) for 30 days. Se concentrations were then measured at set time points (1, 3, 5, 7, 9, 15, and 30 days) by inductively-coupled plasma atomic emission spectrometry (ICP-AES; Varian Vista AX, Santa Clara, CA).

Bacterial assays. *E. coli* (K12 substr. MG1655; ATCC) and *S. aureus* (MRSA252; ATCC) were used to evaluate the anti-

bacterial properties of the TNT-Se samples. Unmodified Ti was used as a control. Both strains of bacteria were propagated in tryptic soy broth (TSB, 30 g L⁻¹, Sigma-Aldrich) for 20 h, and then diluted in TSB to a concentration of 10⁶ colony-forming units (CFU) per ml. To track their colonization by bacteria, each sample was incubated (37 °C, humidified, 5% CO₂) in 2 ml of the bacterial suspension, and the medium was changed every 24 h. At the appropriate treatment time points (1, 3, 5, 7, 9, 15, and 30 days), the samples were gently rinsed three times with PBS (pH 7.4) to remove the non-adherent bacteria. The adherent bacteria on each sample were detached into 2 ml of TSB by ultrasonic vibration (40 W) for 2 min and were serially diluted by 10-fold steps with sterile PBS. Then, 200 μ l of the diluted bacterial suspensions were inoculated onto TSB-agar plates for 24 h at 37 °C, after which the bacterial colonies were counted.

Bacterial membrane morphology. Samples with bacteria were incubated for 24 h for visualization using SEM. The bacteria adhering to the surface were fixed and dehydrated as previously reported,⁴⁶ followed by drying in a critical-point dryer (EMS 850, Electro Microscopy Science Co., Baton Rouge, LA) for surface imaging. The samples were then sputter-coated with gold and observed using an SEM.

Live/dead bacterial assay. Fluorescence confocal microscopy (CLSM, Olympus FluoView FV1000; Germany) and laser scanning cytometry (LSC, CompuCyte iCyte, Waltham, MA) were used to visualize the colonization of bacteria on the samples of interest. Two kinds of bacteria—one Gram-positive (*S. aureus*) and one Gram-negative (*E. coli*)—were inoculated onto samples at 10⁶ CFU ml⁻¹ in TSB. After 24 h of incubation, the medium was removed and cells were stained using the Live/Dead® BacLight™ kit (Invitrogen, Waltham, MA) according to the manufacturer's instructions. Living cells were stained by SYTO 9 (green) while dead cells were stained with propidium iodide (red).

RT-qPCR for *E. coli* gene expression analysis. To examine the mechanism(s) by which the samples influenced bacterial functions, reverse-transcription quantitative PCR (RT-qPCR) was used to track the expression of six relevant *E. coli* genes. All the gene primers and probes were designed using Primer Express software (version 2.0, Applied Biosystems, Waltham, MA). The genes *ompA*, *ompf*, *csaA*, *csaG*, *ahpF*, and *katG* were used to probe different functions of *E. coli* on samples (Table 4), and *ropA* was used as the housekeeping gene. All primers were designed to pair with the TaqMan MGB probe. The homologies of the selected primers and the probe with unrelated sequences were checked by a search with the BLAST program from the National Center for Biotechnology Information (<http://www.ncbi.nlm.nih.gov/BLAST/>).

E. coli grown on samples for 24 h were lysed and homogenized using a PureLink® RNA Mini kit (Invitrogen). The concentration of purified RNA was quantified using a NanoDrop™ 2000/2000c spectrophotometer (Thermo Scientific, Waltham, MA). Then, reverse transcription was carried out with a High Capacity RNA-to-cDNA kit (Invitrogen) using 2 μ g of total RNA

Table 4 Primers and probes for the *E. coli* target and housekeeping genes^a

Gene	Primer	Probe
<i>ompA</i>	F: GGCCTGCAGACTAAATCCA	CGTTTATGGTAAAAACC
	R: AGCGAAGACCGGAGAAACG	
<i>ompF</i>	F: ACACCGATATGCTGCCAGAAT	TGGTGGTGATACTGCATAC
	R: AACACGACCAACGAAGAAGTCA	
<i>csgA</i>	F: TGCAAACCTGATGCCCCGTAAC	CTGACTTGACTATTACCC
	R: CCTGACCAACATCTGCACCAT	
<i>csgG</i>	F: TGCCGACACGCAATACCA	CTCGATCAGATTGCC
	R: ATTGACGACGCGCAGGTT	
<i>ahpF</i>	F: ACAAACTGCGCAGCCTGAA	AACGTCGACATTATTC
	R: TTCCGTGGTTTGGCGATT	
<i>katG</i>	F: GAGCCAATTGCTGACGGTTT	TAACTATCGCGCTCGTCT
	R: CAGTGACTCGGTGGTGAA	
<i>rpoA</i>	F: AGCTGGTCATCGAAATGAAAC	AACGGCACAATCGA
	R: ACGACGAATCGCCTCTTCAG	

^a F, forward; R, reverse.

for each 20 μ l reaction. The cDNA was cooled to 4 $^{\circ}$ C, then 20 μ l reactions with a simplex PCR setup were assembled in the standard 96-well plate setup. Ten microliters of TaqMan Gene Expression Master Mix, 1 μ l of TaqMan gene expression assay solution, and 9 μ l of cDNA template with H₂O were mixed in each well, and the reactions were performed in triplicate for each gene on all 5 samples. Amplification was performed over 40 cycles (denaturing at 95 $^{\circ}$ C for 15 s and annealing extension at 60 $^{\circ}$ C for 1 min) using the QuantStudio[®] 6 Flex Real-Time PCR system. After data acquisition, the relative expression of each gene was calculated using the $\Delta\Delta C_T$ method.

Determination of reactive oxygen species (ROS). The ROS generated by bacteria in the culture medium was determined in terms of malondialdehyde (MDA) equivalents using the TBARS assay (OxiSelect[™] TBARS Assay Kit, Cell Biolabs, Inc., San Diego, CA). *E. coli* (2×10^7 CFU ml⁻¹) were incubated on different samples for 24 h. The bacteria were then detached and re-suspended in PBS *via* sonication on ice. To prevent further oxidation, a BHT solution was added as recommended by the supplier. The absorption of the bacterial solution at $\lambda_{\max} = 532$ nm was used to estimate the formation of TBARS, with analyses carried out in triplicate. The MDA levels were calculated from a calibration of the intensity of TBARS measured at $\lambda = 532$ nm against different concentrations of MDA synthesized by the acidic hydrolysis of 1,1,3,3-tetramethoxypropane.

Macrophage proliferation. Macrophages (RAW 264.7, ATCC TIB-71, Lomianki, Poland) were incubated on the samples in 24-well plates at 1.5×10^4 cells per well in a humidified, 5% CO₂ atmosphere at 37 $^{\circ}$ C. The culture medium was Minimum Essential Medium Alpha (alpha-MEM, Gibco, Waltham, MA) supplemented with 10% fetal bovine serum (FBS, Gibco) and a 1% antibiotic-antimycotic solution (penicillin-streptomycin and fungizone, Gibco). After 24, 48, and 72 h of incubation, macrophage proliferation was measured using an MTS assay (CellTiter 96[®] Aqueous One Solution Cell Proliferation Assay,

Promega, Waltham, MA) according to the manufacturer's instructions.

Statistical analysis. All experiments were conducted in triplicate. Statistically significant differences ($p < 0.05$) were measured using one-way ANOVA combined with the Student–Newman–Keuls *post-hoc* test. Data are expressed as the mean \pm standard deviation.

Conclusions

Different concentrations of Se nanoparticles were incorporated onto and into TiO₂ nanotubes (100–150 nm in diameter). The TNT-Se samples inhibited the growth of both *E. coli* and *S. aureus*, and disrupted the structure and function of the *E. coli* membrane by down-regulating the *ompA* and *ompF* genes. To act against the ROS in bacteria induced by SeNPs, the genes *ahpF* and *katG* of *E. coli* were up-regulated. Moreover, macrophage activity on TNT-Se samples was significantly reduced, suggesting that this material could be used to regulate the inflammatory response. In summary, in the present study we have identified a SeNP-surface modified Ti substrate with the ability to both decrease bacterial functions and potentially control inflammation. Future experiments will be designed to optimize these promising properties for numerous orthopedic and dental applications.

Acknowledgements

The authors thank Northeastern University, the George J. Kostas Nanoscale Technology and Manufacturing Research Center, the National Natural Science Foundation of China (81425007), and the National Basic Science Research Program (2012CB933900) for their support.

References

- 1 L. Zhang and T. J. Webster, *Nano Today*, 2009, **4**, 66–80.
- 2 M. J. Dalby, N. Gadegaard, R. Tare, A. Andar, M. O. Riehle, P. Herzyk, C. D. Wilkinson and R. O. Oreffo, *Nat. Mater.*, 2007, **6**, 997–1003.
- 3 K. G. Neoh, X. Hu, D. Zheng and E. T. Kang, *Biomaterials*, 2012, **33**, 2813–2822.
- 4 N. Wang, H. Li, W. Lu, J. Li, J. Wang, Z. Zhang and Y. Liu, *Biomaterials*, 2011, **32**, 6900–6911.
- 5 J. Park, S. Bauer, A. Pittrof, M. S. Killian, P. Schmuki and K. von der Mark, *Small*, 2012, **8**, 98–107.
- 6 X. Cao, W. Q. Yu, J. Qiu, Y. F. Zhao, Y. L. Zhang and F. Q. Zhang, *J. Mater. Sci. Mater. Med.*, 2012, **23**, 527–536.
- 7 K. C. Popat, L. Leoni, C. A. Grimes and T. A. Desai, *Biomaterials*, 2007, **28**, 3188–3197.
- 8 J. W. Costerton, P. S. Stewart and E. P. Greenberg, *Science*, 1999, **284**, 1318–1322.

- 9 J. Ata-Ali, F. Ata-Ali and F. Ata-Ali, *Int. J. Oral Maxillofac. Surg.*, 2014, **43**, 68–74.
- 10 C. A. Pereira, B. C. Toledo, C. T. Santos, A. C. Pereira Costa, G. N. Back-Brito, E. Kaminagakura and A. O. Jorge, *Diagn. Microbiol. Infect. Dis.*, 2013, **76**, 419–424.
- 11 L. Gendreau and Z. G. Loewy, *J. Prosthodontics*, 2011, **20**, 251–260.
- 12 M. Sinn Aw, J. Addai-Mensah and D. Losic, *Macromol. Biosci.*, 2012, **12**, 1048–1052.
- 13 M. Lai, K. Cai, L. Zhao, X. Chen, Y. Hou and Z. Yang, *Bio-macromolecules*, 2011, **12**, 1097–1105.
- 14 Y. Xin, J. Jiang, K. Huo, T. Hu and P. K. Chu, *ACS Nano*, 2009, **3**, 3228–3234.
- 15 Y. H. Lee, G. Bhattarai, I. S. Park, G. R. Kim, G. E. Kim, M. H. Lee and H. K. Yi, *Biomaterials*, 2013, **34**, 10199–10208.
- 16 G. M. Soares, L. C. Figueiredo, M. Faveri, S. C. Cortelli, P. M. Duarte and M. Feres, *J. Appl. Oral Sci.*, 2012, **20**, 295–309.
- 17 J. M. ten Cate and E. Zaura, *Adv. Dent. Res.*, 2012, **24**, 108–111.
- 18 W. Liu, P. Su, S. Chen, N. Wang, Y. Ma, Y. Liu, J. Wang, Z. Zhang, H. Li and T. J. Webster, *Nanoscale*, 2014, **6**, 9050–9062.
- 19 L. Zhao, H. Wang, K. Huo, L. Cui, W. Zhang, H. Ni, Y. Zhang, Z. Wu and P. K. Chu, *Biomaterials*, 2011, **32**, 5706–5716.
- 20 K. Vasilev, V. Sah, K. Anselme, C. Ndi, M. Mateescu, B. Dollmann, P. Martinek, H. Ys, L. Ploux and H. J. Griesser, *Nano Lett.*, 2010, **10**, 202–207.
- 21 W. Liu, P. Su, A. Gonzales 3rd, S. Chen, N. Wang, J. Wang, H. Li, Z. Zhang and T. J. Webster, *Int. J. Nanomed.*, 2015, **10**, 1997–2019.
- 22 P. A. Tran and T. J. Webster, *Int. J. Nanomed.*, 2011, **6**, 1553–1558.
- 23 Q. Wang, P. Larese-Casanova and T. J. Webster, *Int. J. Nanomed.*, 2015, **10**, 2885–2894.
- 24 J. Yang, K. Huang, S. Qin, X. Wu, Z. Zhao and F. Chen, *Dig. Dis Sci.*, 2009, **54**, 246–254.
- 25 M. Shakibaie, H. Forootanfar, Y. Golkari, T. Mohammadi-Khorsand and M. R. Shakibaie, *J. Trace Elem. Med. Biol.*, 2015, **29**, 235–241.
- 26 X. Huang, X. Chen, Q. Chen, Q. Yu, D. Sun and J. Liu, *Acta Biomater.*, 2016, **30**, 397–407.
- 27 C. H. Yun, J. S. Yang, S. S. Kang, Y. Yang, J. H. Cho, C. G. Son and S. H. Han, *Int. Immunopharmacol.*, 2007, **7**, 1192–1198.
- 28 H. Vunta, B. J. Belda, R. J. Arner, C. Channa Reddy, J. P. Vanden Heuvel and K. Sandeep Prabhu, *Mol. Nutr. Food Res.*, 2008, **52**, 1316–1323.
- 29 P. A. Tran, N. O'Brien-Simpson, E. C. Reynolds, N. Pantarat, D. P. Biswas and A. J. O'Connor, *Nanotechnology*, 2016, **27**, 045101.
- 30 R. K. Dutta, B. P. Nenavathu and S. Talukdar, *Colloids Surf., B*, 2014, **114**, 218–224.
- 31 A. W. Confer and S. Ayalew, *Vet. Microbiol.*, 2013, **163**, 207–222.
- 32 E. Sugawara and H. Nikaïdo, *J. Biol. Chem.*, 1992, **267**, 2507–2511.
- 33 C. Ambrosi, M. Pompili, D. Scribano, C. Zagaglia, S. Ripa and M. Nicoletti, *PLoS One*, 2012, **7**, e49625.
- 34 J. Zhou, K. Wang, S. Xu, J. Wu, P. Liu, G. Du, J. Li and J. Chen, *J. Proteomics*, 2015, **113**, 15–28.
- 35 S. Kojima and H. Nikaïdo, *J. Biol. Chem.*, 2014, **289**, 26464–26473.
- 36 M. Hammar, A. Arnqvist, Z. Bian, A. Olsen and S. Normark, *Mol. Microbiol.*, 1995, **18**, 661–670.
- 37 L. Cremet, S. Corvec, E. Batard, M. Auger, I. Lopez, F. Pagniez, S. Dauvergne and N. Caroff, *Diagn. Microbiol. Infect. Dis.*, 2013, **75**, 252–255.
- 38 M. M. Barnhart and M. R. Chapman, *Annu. Rev. Microbiol.*, 2006, **60**, 131–147.
- 39 L. S. Robinson, E. M. Ashman, S. J. Hultgren and M. R. Chapman, *Mol. Microbiol.*, 2006, **59**, 870–881.
- 40 H. Loferer, M. Hammar and S. Normark, *Mol. Microbiol.*, 1997, **26**, 11–23.
- 41 J. Kim, Y. Cho, I. A. Jang and W. Park, *Appl. Microbiol. Biotechnol.*, 2015, **99**, 10611–10626.
- 42 L. C. Seaver and J. A. Imlay, *J. Bacteriol.*, 2001, **183**, 7182–7189.
- 43 H. R. Panek and M. R. O'Brian, *J. Bacteriol.*, 2004, **186**, 7874–7880.
- 44 B. A. Carlson, M. H. Yoo, Y. Sano, A. Sengupta, J. Y. Kim, R. Irons, V. N. Gladyshev, D. L. Hatfield and J. M. Park, *BMC Immunol.*, 2009, **10**, 57.
- 45 J. Wang, Y. Zhang, Y. Yuan and T. Yue, *Food Chem. Toxicol.*, 2014, **68**, 183–189.
- 46 H. Hu, W. Zhang, Y. Qiao, X. Jiang, X. Liu and C. Ding, *Acta Biomater.*, 2012, **8**, 904–915.